Simultaneous Optimization of Shape and Topology of Free-form Shells Based on Uniform Parameterization Model

Yi XIA[a,b] , Yue WU[*a], Max A.N. Hendriks[b,c]

[a] Key Lab of Structures Dynamic Behavior and Control of China Ministry of Education, Harbin Institute of Technology, Harbin 150090, PR China

[b] Faculty of Civil Engineering & Geosciences, Delft University of Technology, Steinweg 1, 2628CN Delft, The Netherlands

[c] Department of Structural Engineering, Norwegian University of science and technology (NTNU), Rich. Birkelandsvei 1A, 7491 Trondheim, Norway

E-mail address: wuyue_2000@163.com

Address: School of Civil Engineering, Harbin Institute of Technology, P.O. Box 2619, 202 Haihe Road, Harbin, China, 150090

Abstract

In current optimization methods for free-form shells, the shape and topology are usually optimized separately. These methods are based on the assumption that the shape and topology of a shell influence each other only slightly, but this is not always correct. Moreover, different parameterization models are used in the shape optimization and topology optimization of free-form shells, which brings difficulties to carry out the integrated optimization. To solve this problem, an integrated method is proposed for simultaneously optimizing shape and topology for free-form shells. A uniform parameterization model based on NURBS solids is established to parameterize the free-form shells. In this model, only a small number of variables are used to describe both the shape and topology of the shell. In this way, the integrated optimization problem can be simplified, thus decrease the computational complexity. The integrated optimization of shape and topology ~~integrated optimization~~ is a complicated and large-scale optimization problem. Solving this problem requires a suitable optimization method. In this paper, the Method of Moving Asymptotes (MMA) is adopted. Finally, numerical examples are presented to address the importance of the optimization sequences and show the effectiveness and application of the proposed method.

Keywords:

Integrated optimization; Free-form shell; Uniform parameterization model; Shape optimization; Topology optimization; NURBS;

1. Introduction

One of the ultimate aims of the structural engineers is to design safe and economical structures. Among different types of structures, shells are mechanical efficient. Benefitting of the excellent structural behavior, shells are always light weight structures. Engineers and architects, attracted by its elegance and aesthetic performance [1], even called the shells the structural “prima donna” [2]. Among the shells, free-form shells are favored for their rich architectural expressions and excellent performances. But sometimes their irregular shapes may result in a bad structural behavior. A sub-working group of the International Association for Shell and Spatial Structures (IASS) [3] emphasized the importance of the shape design for free-form shells. To solve this problem, a series of methods to find shells with better structural behavior were proposed. In the early time, the shape of shells was found through experimental methods, such as the soap film method [4] and the hanging method [5]. In recent decades, numerical methods for improving the structural behavior of shells has become the dominant research method.

Stress distribution within shells is the most important aspect affecting the structural performance. Triangular stress distributions in the cross section lead to unfavorable mechanics of shells; the stress distribution should be as uniform as possible in optimized shells [6]. The more the stress state resembles a membrane stress state, the better is the performance of shells. Changing shell shapes mainly affects the stress distribution, thus many researchers proposed the shape optimization method to improve the structural capacity. Bletzinger and Ramm proposed a structural optimization method to optimize the shape of shells [7]. Next, they investigated the differences in shapes of shells generated by different methods, such as the hanging method, the soap film method and a structural optimization based method [8]. A common conclusion was that optimization methods are a generalization of the form finding methods [9]. A comparative review of the optimization methods for shells and their relationship to form finding methods was given in [10]. In some cases, it was noticed that even slight changes of the shape of shells had important improvements of the structural behavior [11].

To solve a structural optimization problem, there are three important parts. In terms of the mechanics in the optimization process, usually, the finite element method (FEM) is used. Researchers used programs like NASTRAN, MSC/NASTRAN, ADINA and ANSYS [1, 12-16].

Different optimization algorithms are considered in the mathematical part, such as the gradient based method [17], the genetic algorithm [18-19] and the firefly algorithm [20]. Finally, different parameterization methods were proposed. For example, in [14] a major node method was proposed to parameterize the shape of shells and reducing the number of variables in the optimization process. In [21] a non-parametric based method was proposed for optimizing the shape of free-form shells.

Topology optimization of shells received relatively limited attention by researchers, compared to shape optimization of shells. In [22], a method to optimize the shape and thickness of free-form shells was proposed. In the method, a linear interpolation of nodal thickness variables was used, which avoided discontinuities of thicknesses within and between elements. The integrated optimization of shells, considering the shape and topology optimization was investigated in [23-25]. With the progress of the 3D printing construction technology, the construction of complex forms becomes possible [26]. To fully exploit this technology, more investigations of the integrated optimization of free-form shells are required.

Usually, the shape optimization and topology optimization were two separate processes in the shell optimization design. The shape of shells was optimized while maintaining the topology. In [12], it was concluded that the optimized shape of shells was sensitive to their topology, and the change of the shell topology resulted in different optimized shapes. The two optimization problems are connected; the optimal result could not be obtained by divided optimizations [23-25]. To obtain more optimized results, the simultaneous optimization approach for shells is required. The approach needs to be elaborated to prevent wrong results due to interaction of shape and topology. Usually, researchers used different parameterization models for describing the shape and topology of free-form shells, which brings difficulties to integrate the two optimization procedures in one method. This paper focuses on developing a suitable and uniform approach for the integrated shape and topology optimization of free-form shells.

In this paper, a uniform parameterization method is established to describe the geometry of the shell. Based on this parameterization method, a shape and topology integrated optimization method of free-form shells is proposed. In the geometry part, the Non-Uniform Rational Basis Spline (NURBS) function is selected as the basic function to formulate the uniform

parameterization model. Usually, NURBS surfaces are used in the shape optimization of shells [19, 20, 22, 25]; Here NURBS solids are used as an alternative. The geometry data is stored in a few control points, the dimension of NURBS can be easily extended to allow more design freedom. The control points are used to adjust the geometry of the free-form shells and are used as the variables in the optimization process. In the mathematical part, the Method of Moving Asymptotes (MMA) [27] is used to solve the integrated optimization problem of minimizing the strain energy of shells with a volume constraint. It was concluded that accounting for minimizing strain energy is an implicit way of improving the structural behavior in the optimization of shells [1]. ANSYS software is used to solve the mechanic problem. By combining the three parts together, the shape and topology integrated optimization method is established.

The paper comprises four sections. After the introduction section, the second section describes the methodology. It contains the establishment of the uniform parameterization model, the transformation method of different parameterization models and the framework of the integrated optimization method. The third section includes numerical examples. They are tested and discussed to illustrate the effectiveness of the proposed method. The last section presents the conclusions of this paper.

2. Methodology

2.1 Uniform parameterization model

2.1.1 Basis and notations

A NURBS solid is a type of embedding volume. The fundamentals of NURBS in [30] are summarized here. A NURBS solid is a piecewise polynomial solid based on weighted control points. The basic NURBS function $N_{i,p}(\xi)$ is decided by knot vectors $\Xi \in \{\xi_0, \xi_1, \ldots, \xi_{m+p}\}$, where p is the degree, i is the index of the control points, ξ is a real number called the knot and m is the number of control points. An interval $[\xi_i, \xi_{i+1}]$ is called a knot span and the whole patch is $[\xi_0, \xi_{m+p}]$. The *k-th* repeated times of knots decide the continuity by C^{p-k}. Then, the basis function $N_{i,p}(\xi)$ can be defined as in Eq. (1).

$$\begin{cases} N_{i,0}(\xi) = \begin{cases} 1, & \text{if } \xi_i \le \xi < \xi_{i+1} \\ 0, & \text{others} \end{cases} \\ N_{i,p}(\xi) = \dfrac{\xi - \xi_i}{\xi_{i+p} - \xi_i} N_{i,p-1}(\xi) + \dfrac{\xi_{i+p+1} - \xi}{\xi_{i+p+1} - \xi_{i+1}} N_{i+1,p-1}(\xi) \end{cases} \tag{1}$$

By the linear combination of control points $\mathbf{P}_i$, weights $\mathbf{W}_i$ and basic functions $N_{i,p}(\xi)$, the NURBS solids can be computed. For compact notation, the function R is defined in Eq. (2), the NURBS solid can be calculated in Eq. (3).

$$R_{ijk}(\xi,\eta,\omega) = \frac{[N_{i,p_1}(\xi)N_{j,p_2}(\eta)N_{k,p_3}(\omega)]\mathbf{W}_{ijk}}{\sum\sum\sum[N_{i,p_1}(\xi)N_{j,p_2}(\eta)N_{k,p_3}(\omega)]\mathbf{W}_{ijk}} \tag{2}$$

In terms of the NURBS solid, it can be generated by the three-order tensor product of the knot vectors ($\xi \in \Xi_1$, $\eta \in \Xi_2$ and $\omega \in \Xi_3$), shown in Eq. (3). The $m_1 \times m_2 \times m_3$ control points $\mathbf{P}_{ijk}$ $(i = 1 \ldots m_1,\ j = 1 \ldots m_2$ and $k = 1 \ldots m_3)$ form the control point polyhedron, the orders of NURBS basic functions defined on three knot vectors are p_1, p_2 and p_3 respectively. The NURBS solid representing a shell in the physical and parametric space is shown in Fig. 1. In the NURBS model, index m_3 in the control point polyhedron is 2, and there is only one knot span in $\omega \in \Xi_3$ to represent the topology of shell elements.

$$\boldsymbol{E}(\xi,\eta,\omega) = \sum_{i=1}^{m_1}\sum_{j=1}^{m_2}\sum_{k=1}^{m_3} R_{ijk}(\xi,\eta,\omega)\mathbf{P}_{ijk} \tag{3}$$

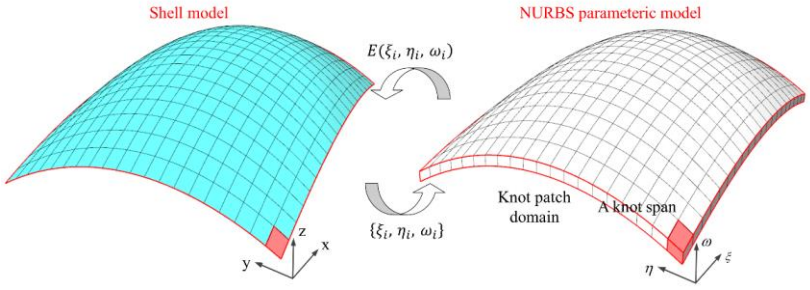

Fig. 1. The NURBS parametric model and the represented shell

2.1.2 Geometry parameterization of free-form shells

NURBS haves been used previously to parameterize the shape of shells' ~~shape~~ in the shape

optimization process ~~in~~ [19, 20, 22, 25]. In this paper, in Eq. (3), the parameters define the geometry including the shape and the topology of free-form shells. The order of NURBS basic functions affects the continuity. Using more control points in parameterizing a shell, ~~on the one hand more~~increases the number of optimization variables ~~are provided~~within in the optimization process, ~~on the other hand the optimized result could be different (see discussions in Section 3.5.3)~~and thus allows for more freedom in describing the shape and topology. For shells, the thickness is much smaller than the other sizes. The other parameters are set to satisfy the demand in describing the shape of the shells. The finite element analysis model is generated according to the design parameterization model. ~~How to~~The mesh used in the finite element analysis ~~model~~ could affect the analysis result. I~~, i~~n this paper ~~the structural~~ uniform meshes with shell elements are~~is~~ used ~~for shells~~. In order to obtain the aimed meshes from the parameterization model, uniform knots in the parameterization model are adopted, each knot in the parameterization model represents the node in the analysis model, and knot spans denotes structural elements. The thickness of the knot denotes the density of the element which can be used in the topology optimization.

Minimizing the difference between the parameterization model and the analysis model is important. Fig. 2. is an example of analysis models based on one parameterization model with different knot spans. It shows that the difference between two models can be decreased to an acceptable level by increasing knot spans.

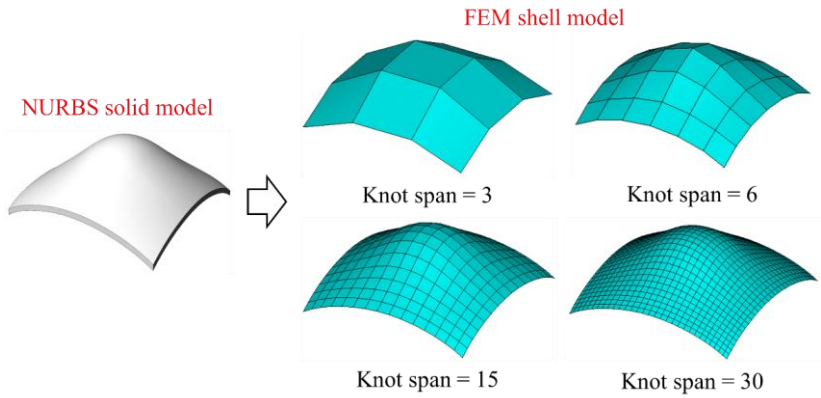

Fig. 2. Analysis models based on the same parameterization model with different knot spans

Fig. 3 shows an example of adjusting the geometry of a shell by changing control points in the

parameterization model. In the figure, $\mathbf{P}_{ijk}$ are the control points of the parameter model. The shape can be changed through $\mathbf{P}_{ijk} + \Delta s$ and changing the thickness by $\mathbf{P}_{ijk} \pm \Delta t$. By increasing Δt, a void area in the parameter model appears, which leads to a hole in the FEM model. In this paper, a minimal thickness is assigned to elements in a hole with a small Young's modulus to prevent singularity in the analysis. The black and gray areas in the thickness contour of the FEM model indicate solid parts and the white areas indicate void. In this way, the NURBS-based model is taken as the common basis to parametrize the shape and topology of a shell. Besides, the change of the shape by varying the shape model doesn't affect variables in the topology model. The shape of structures is decided by the mid-surface of the shape model whereas the topology is the result of the difference of control variables of the topology model. Both the shape and topology are determined and changed implicitly by the control points of the parameterization model.

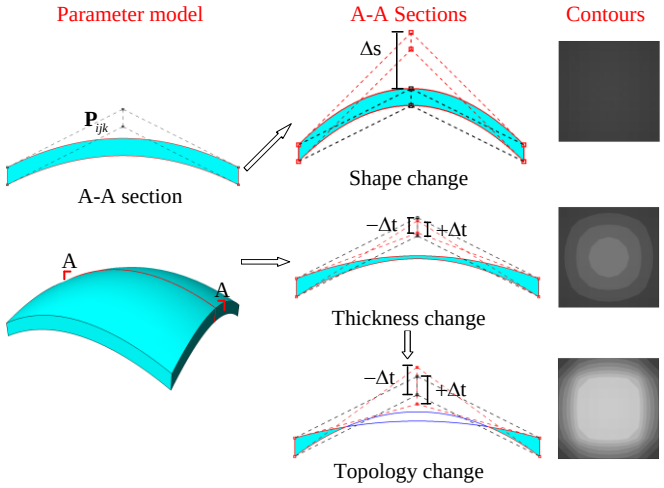

Fig. 3. Adjusting a parametric model through control points

Customarily, the number of variables in the topology optimization ~~relates~~ defines to the structural meshes [31]. The huge number of un-coupled variables causes the problem of mesh instability in the topology optimization [28]. The noise clean technique is adopted for this kind of problem [25]. Taking advantages of the parameterization model, only a small number of control points is used to describe the geometry of shells and taken as optimization variables. Besides, the continuity of the model provides smoothness between each element, which prevents the mesh instability problem in

an implicit way [28]. When the thickness of the shell elements is lower than a threshold value, the material in those areas is interpreted as insignificant. The thickness optimization in a broad sense is also a way of the topology optimization and it leads to more optimal result than topology optimization [29]. In this paper, the minimum thickness is assigned as 1% of the original thickness.

2.2 Transformation method of parameterization models

As we know, the number of variables will influence the computational costs and optimization results. According to the uniform parameterization model in Section 2, the number of shape variables equals to the number of topology variables. In this section, a method of parameterizing the same shell with different parameterization models is established. It enables that the number of variables changes during the optimization, which gives extra flexibility considering efficiency and effectiveness in optimization processes. More specifically, different NURBS solids will be used for shape and topology (or thickness) optimization, both representing the same shell structure. The most important point is that all parameterization models should describe the same geometry of a shell, or the structural analysis results could be different in terms of the shape parameterization model and the topology parameterization model. For establishing different parameterization models while maintaining the same geometry, the transformation method based on NURBS Global Interpolation [30] is introduced.

Commented [MH1]: I do not understand this part. Maybe you can skip it.

The parameters of the original model with $n_1 \times n_2 \times n_3$ nodes are set as, the orders (p_1, p_2, p_3), control point polyhedron $\mathbf{P}_{ijk}$ $(i = 1...m_1,\ j = 1...m_2$ and $k = 1...m_3)$ and uniform knot values $(\xi_i, \eta_j, \omega_k)$ $(i = 1...n_1,\ j = 1...n_2, k = 1...n_3)$. Then the parameters of the new model are control points $\bar{\mathbf{P}}_{ijk}$ $(i = 1...\bar{m}_1,\ j = 1...\bar{m}_2$ and $k = 1...\bar{m}_3)$, orders $(\bar{p}_1, \bar{p}_2, \bar{p}_3)$ and uniform values $(\bar{\xi}, \bar{\eta}, \bar{\omega})$ on the new knot vectors. The values of $\bar{\mathbf{P}}_{ijk}$ are required and calculated as follows.

Firstly, the node data of the new model is calculated in Eq. (4) and is known. Solving this equation directly is complex. Since $\mathbf{E}(\bar{\xi}, \bar{\eta}, \bar{\omega})$ is the tensor product result, $\bar{\mathbf{P}}_{ijk}$ can be calculated in a simpler way by a sequence of surface interpolations followed by curve interpolations.

$$\mathbf{E}(\bar{\xi},\bar{\eta},\bar{\omega})=\sum_{i=1}^{\bar{m}_1}\sum_{j=1}^{\bar{m}_2}\sum_{k=1}^{\bar{m}_3}R_{ijk}(\bar{\xi},\bar{\eta},\bar{\omega})\bar{\mathbf{P}}_{ijk} \tag{4}$$

Secondly, the Eq. (4) can be written as Eq. (5), where $\mathbf{Q}_{ij}(\bar{\omega})=\sum_{k=1}^{\bar{m}_3}R_k(\bar{\omega})\bar{\mathbf{P}}_{ijk}$. It shows that the solid is interpolated by surfaces with varying parameters $\bar{\omega}$.

$$\mathbf{E}(\bar{\xi},\bar{\eta},\bar{\omega})=\sum_{i=1}^{\bar{m}_1}\sum_{j=1}^{\bar{m}_2}R_{ij}(\bar{\xi},\bar{\eta})[\sum_{k=1}^{\bar{m}_3}R_k(\bar{\omega})\bar{\mathbf{P}}_{ijk}]=\sum_{i=1}^{\bar{m}_1}\sum_{j=1}^{\bar{m}_2}R_{ij}(\bar{\xi},\bar{\eta})\mathbf{Q}_{ij}(\bar{\omega}) \tag{5}$$

Thirdly, the Eq. (5) can be transformed as Eq. (6), where $\mathbf{T}_i(\bar{\eta})|_{\bar{\omega}}=\sum_{j=1}^{\bar{m}_2}R_j(\bar{\eta})\mathbf{Q}_{ij}(\bar{\omega})$. It means that the interpolation surfaces of the fixed parameter $\bar{\omega}$ can be interpolated by curves with varying parameters $\bar{\eta}$.

$$\sum_{i=1}^{\bar{m}_1}\sum_{j=1}^{\bar{m}_2}R_{ij}(\bar{\xi},\bar{\eta})\mathbf{Q}_{ij}(\bar{\omega})=\sum_{i=1}^{\bar{m}_1}R_i(\bar{\xi})[\sum_{j=1}^{\bar{m}_2}R_j(\bar{\eta})\mathbf{Q}_{ij}(\bar{\omega})]=\sum_{i=1}^{\bar{m}_1}R_i(\bar{\xi})\mathbf{T}_i(\bar{\eta})|_{\bar{\omega}} \tag{6}$$

Fourthly, by solving three simpler linear equations the required control points $\bar{\mathbf{P}}_{ijk}$ can be obtained. Solving the Eq. (6) in advance, curve control points $\mathbf{T}_i(\bar{\eta})|_{\bar{\omega}}$ with fixed $\bar{\omega}$ can be calculated. Then subtitute the result in $\mathbf{T}_i(\bar{\eta})|_{\bar{\omega}}=\sum_{j=1}^{\bar{m}_2}R_j(\bar{\eta})\mathbf{Q}_{ij}(\bar{\omega})$, surface control points $\mathbf{Q}_{ij}(\bar{\omega})$ are calculated.

Finally, the control points $\bar{\mathbf{P}}_{ijk}$ are computed by solving $\mathbf{Q}_{ij}(\bar{\omega})=\sum_{k=1}^{\bar{m}_3}R_k(\bar{\omega})\bar{\mathbf{P}}_{ijk}$. The procedure of transforming a shell parametric model is shown in Fig. 4. In the figure, (a) shows the node data of the original model, (b) the interpolated surfaces, (c) the interpolated curves based on the surfaces, (d), (e) and (f) are the solving steps to calculate interpolated points of curves, surfaces and finally the required shell parametric model.

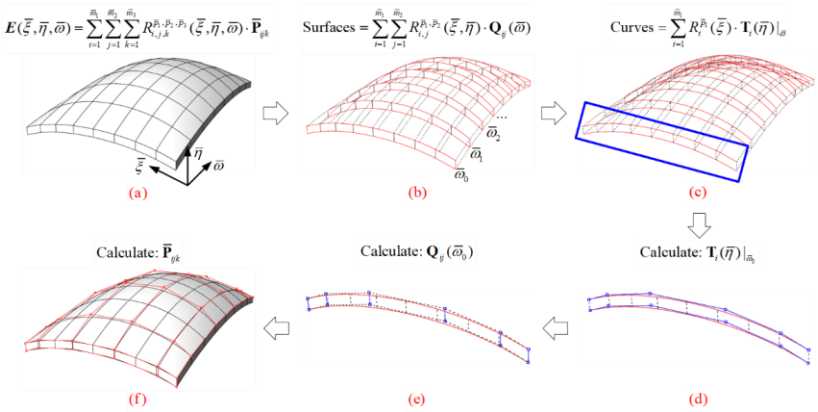

Fig. 4. The procedure of transforming a shell parametric model

Due to the analytical difference of the interpolation process, the new models based on this method lead to ~~the~~ a geometrical dissimilarity ~~y difference from~~ compared to the original model. However, the difference can be kept within a small range. An example in Fig. 5 shows analysis models based on the different parameterization models. The original model has $5\times5\times2$ control points with orders $(2, 2, 1)$ and 30×30 knot spans. In figure (a), the number of control points increases, the average difference of the nodal coordinates comparing with ones of the original analysis model is about 0.01%. In figure (b) the orders increase. In figure (c) the orders decrease to create the model, obviously large differences occur. By increasing the number of control points in (e), the difference is reduced. In figure (d) both the number of control points and orders are increased.

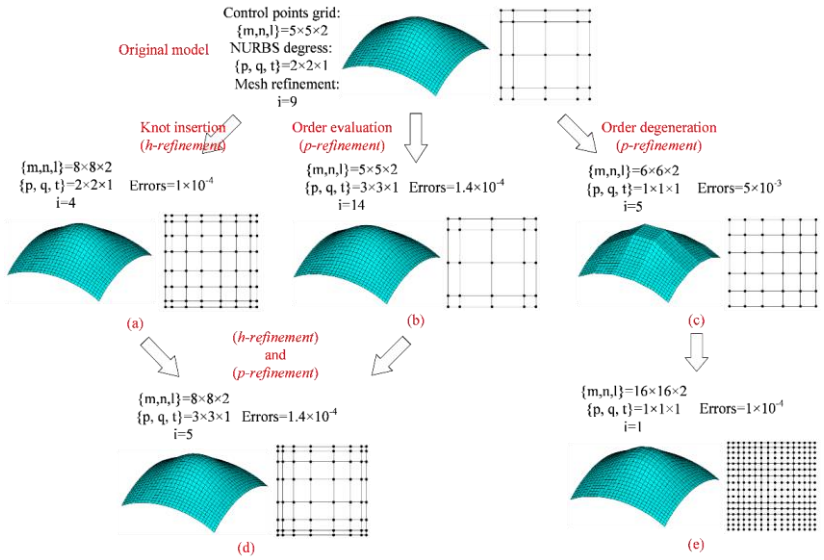

Fig. 5. Different models transformed from the original one

2.3 Framework of the integrated optimization method

The establishment of a mathematical model of the optimization problem is shown in Eq. (7).

$$\begin{cases} \text{find: } \mathbf{X}_k = (\mathbf{S}_k, \mathbf{T}_k) \\ \text{min: } f(\mathbf{X}_k) = SE(\mathbf{X}_k) \\ \text{s.t.: } V(\mathbf{T}_k) \le V_{\max} \quad , t_{\min} \le t_i(\mathbf{T}_k) \le t_{\max}, \\ \quad \mathbf{S}_{\min} \le \mathbf{S}_k \le \mathbf{S}_{\max}, \mathbf{T}_{\min} \le \mathbf{T}_k \le \mathbf{T}_{\max} \end{cases} \tag{7}$$

Where, $\mathbf{X}_k$ are the optimization variables of the k-th step, consisting of shape variables $\mathbf{S}_k$ and topology variables $\mathbf{T}_k$. The variations of shells can be seen in Fig. 3, where the Δt and Δs for different control points forms the vectors $\mathbf{S}_k$ and $\mathbf{T}_k$ respectively. In this paper, only the Z-direction coordinates of the control points are optimized. The objective function $f(\mathbf{X}_k)$ is the structural strain energy $SE(\mathbf{X}_k)$. In the topology optimization process, the SIMP material model with penalty *h* [31] is adopted combined with the density variables $t_i(\mathbf{T}_k)$ of the i-th element to modify the Young's modulus, shown in Eq.(8). The variables can be calculated through the thickness as shown in Fig. 3. $V(\mathbf{T}_k)$ is the volume constraints of the shell.

$$\bar{E} = E_0 \left[t_i(\mathbf{T}_k) \right]^h \tag{8}$$

In the parameterization model, the topology density $t_i(\mathbf{T}_k)$ of the i-th element is decided by variables $\mathbf{T}_k$, thus it brings the difficulty to find the distinct topology optimization result. Reducing the coupling of the densities is of importance. The adaptive constraints for topology variables and the filter ϕ of the $t_i(\mathbf{T}_k)$ are proposed to solve this problem. The filter is shown in Eq. (9). It is the smooth Heaviside step function, where boundaries are $t_{\max}$ and $t_{\min}$, ε is the value of the smooth area. In this way, density constraints $t_{\min} \le t_i(\mathbf{T}_k) \le t_{\max}$ in the Eq. (8) can be simplified. The adaptive constraints with the varying boundaries of topology variables are as follows in the k-th step $\mathbf{T}_{\max}(\mathbf{T}_{\min}) = \mathbf{T}_{\max,\text{initial}}(\mathbf{T}_{\min,\text{initial}}) \pm \beta k$ where β is 0.1 in this paper.

$$\bar{t}_i = \phi(t_i, t_{\max}, t_{\min}, \varepsilon)$$

$$\bar{t}_i = \begin{cases} t_{\min} + \varepsilon \cdot \dfrac{1}{\mathrm{e}^{(t_{\min}+\varepsilon-t_i)/\varepsilon}}, & t_{\min} \le t_i \le t_{\min} + \varepsilon \\ t_i, & t_{\min} + \varepsilon < t_i < t_{\max} - \varepsilon \\ t_{\max} - \varepsilon \cdot \dfrac{1}{\mathrm{e}^{(t_i+\varepsilon-t_{\max})/\varepsilon}}, & t_{\max} - \varepsilon \le t_i \le t_{\max} \end{cases} \tag{9}$$

The shape and topology integrated optimization ~~is the~~amounts to a complicated and large-scale optimization problem. The MMA method [27] is used in this paper. Based on sequential convex programming, this optimization method can solve the complex optimization problem by solving a sequence of explicit and convex approximated sub-problems. Using MMA optimization method to update the optimization variables, the sensitivities of the variables are required. In this paper, ~~due~~ considering the ~~o a~~ small number of optimization variables and ~~simplicity in~~the ease of implementing, the first-order forward finite difference method is used to calculate the sensitivities for the objective function and the constraint function, written as Eq. (10). There are some differences of shape variables and topology variables, such as the magnitude of allowable variation. The large difference may result in numerical errors of the result. To solve this problem, the scaling technique is utilized in [25]. However, in this paper it is not necessary to scale the variables. The difference of results is slight, which means these two types of variables are nearly independent. The verification is discussed in Section 3.5.1.

$$\frac{\partial f}{\partial x_i} \approx \frac{f(x + \Delta x_i) - f(x)}{\Delta x_i} \tag{10}$$

Finally, summarizing Section 2, a method is proposed to optimize free-form shells. The flowchart is shown in Fig. 6. The terminatione condition is that the difference of two-step values of the objective function is smaller than a given ~~minimum number~~tolerance, which ~~denotes~~ indicates that a stable optimized result is obtained.

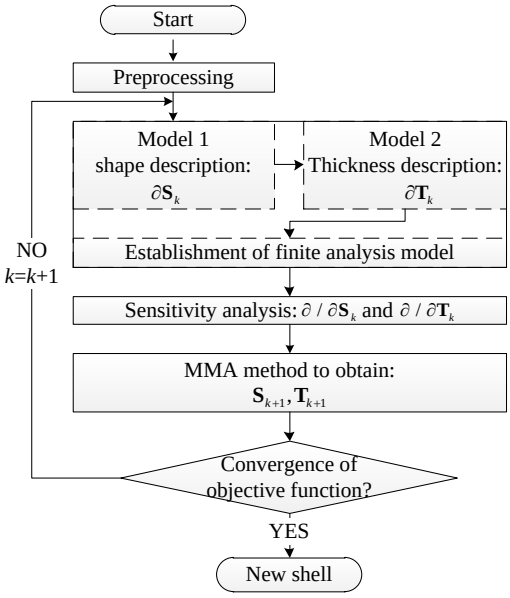

Fig. 6. The procedure of the integrated optimization method

3. Numerical examples and discussions

In this section, several numerical examples are presented to verify the proposed method. The important factors of this method are illustrated through the discussion. In these examples, the triangular elastic shell elements considering both in-plane and out-of-plane states are used. The parameters of the MMA optimizer are at default settings as in [27].

3.1 Example one

This shell is simply supported by four corners and subject to a concentrated load F=10kN. The Young's modulus of the material is 2×10^9 Pa and the Poisson's ratio is 0.3, the span of the shell is 6 m, the original rise is 0.45 m, and the original thickness is 0.1 m. The original geometry of the shell is shown in Fig. 7.

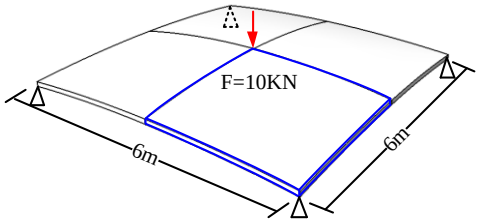

Fig. 7. The original shell

Taking the advantages of the structural symmetry, the shell within blue lines in Fig. 7. is analyzed and optimized. Two parameterization models are established, in the shape optimization the model is constructed by $4\times4\times2$ control points with the order $(3,3,1)$, and in the topology optimization it is constructed by $7\times7\times2$ control points with the order $(2,2,1)$. The original FEM analysis model of 20×20 meshes are shown in Fig. 8.

There are 10 shape variables and 28 topology variables in this optimization problem, shown as red points in Fig. 8. The number of the variables in the optimization process is independent of the FEM meshes. In the traditional density-based topology optimization method, each element has an optimization variable which may cause the instability problem in the result. Here, the continuity of the parameterization model provides the continuous changes between the elements, which prevent the mesh instability problem in an implicit way.

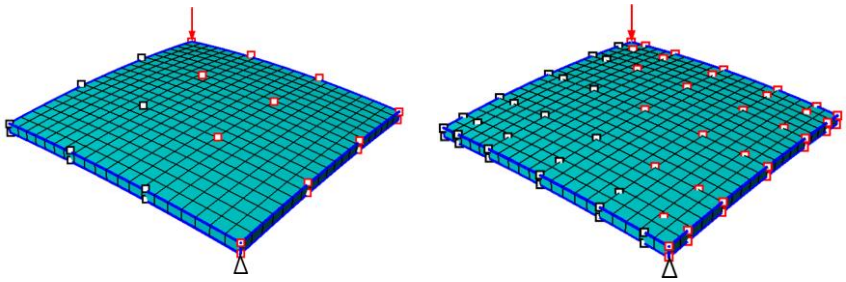

(a) Shape optimization parametric model (b) Topology optimization parametric model

Fig. 8. Two parameterization models

In the optimization process, the maximum shape change is 1.5 m, and the max volume is limited to be less than the half of the original volume. The convergence analysis of the finite difference approximations is presented in Fig. 9. It has the stable region of the finite difference from 10^{-3} to 10^{-7}, in the present case the finite differences were set to 10^{-4}. Fig. 10 shows the history of the

shape and topology optimization including some snapshots of topology contours. The total strain energy reduces to 31.76 Nm after 70 optimization steps.

Fig. 11 shows the optimum shell after the shape and topology optimization, which appears like a four-bar truss structure. Moreover, the shape of the optimized shell shows zero-order smoothness (i.e. C^0 continuous) across the two lines of symmetry. This is a result of the applied NURBS. An optimization taking the complete shell as point of departure would clearly have resulted in another shape. Note that appropriate boundary conditions have been selected in the finite element model, representing the symmetry in a mechanical sense. The calculated displacement field is thus first-order smooth across the lines of symmetry and the obtained shape of Fig. 11 is a valid result.

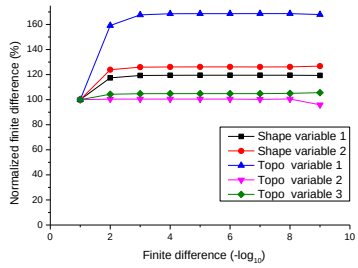

Fig. 9. Convergence analysis of the finite difference approximations

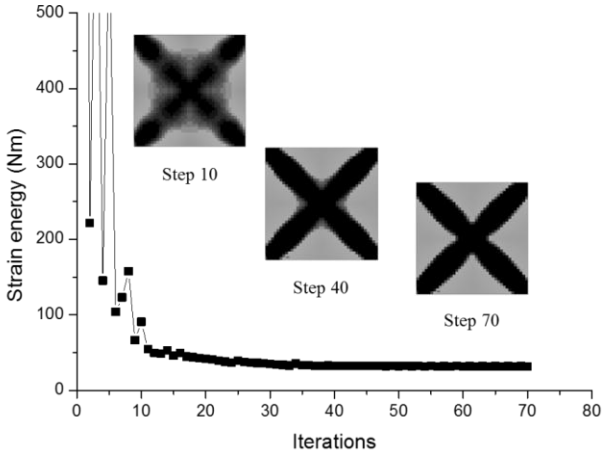

Fig. 10. The history of the shape and topology optimization

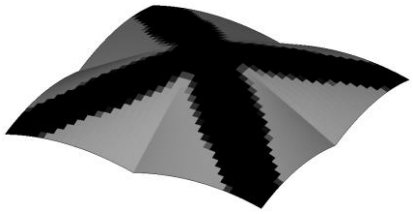

Fig. 11. The geometry after the shape and topology optimization

3.2 Example two

The shell in this example has the same parameters as the first example, but with different load and support conditions, as shown in Fig. 12. The convergence analysis of the finite difference approximations is shown in Fig. 13. Similar with results of Example one, it has a stable region for finite differences from 10^{-3} to 10^{-8}; the finite difference in this example is set to 10^{-4}.

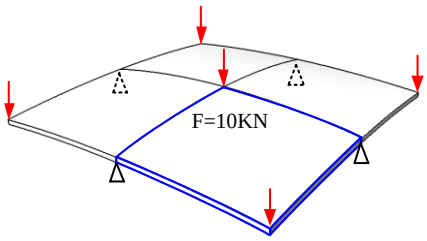

Fig. 12. The original shell

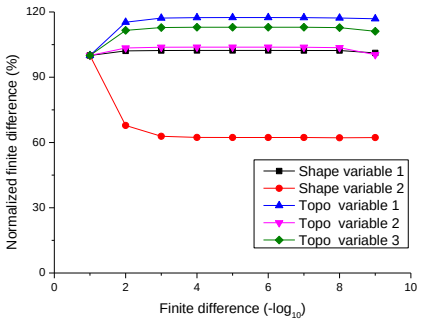

Fig. 13. Convergence analysis of the finite difference approximations

Fig. 14 shows the history of the shape and topology optimization and some snapshots of the contours. In this example, the minimal strain energy reduces to about 155.1 Nm after 90 optimization steps. Fig. 15 shows the shell after the shape and topology optimization.

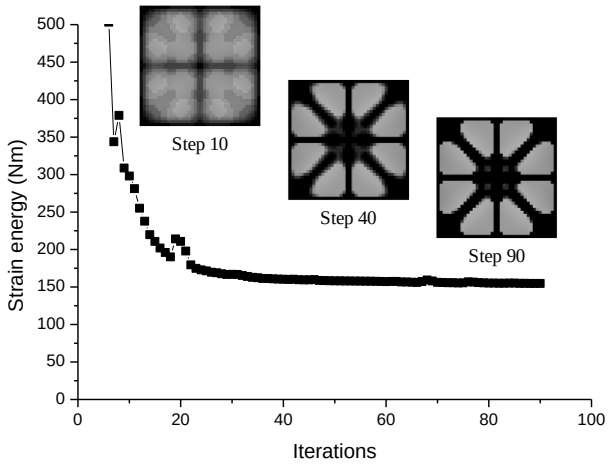

Fig. 14. The history of the shape and topology optimization

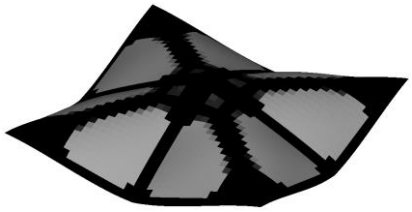

Fig. 15. The geometry after the shape and topology optimization

3.3 Example three

This example aims to optimize an irregular shell by changing the shape and finding the distribution of a reinforced layer at the bottom of the shell. The original geometry of the irregular shell is shown in Fig. 16. The span of the shell is 13 m, the rise is 0.8 m, and the thickness of the shell and the reinforced material is 0.1 m and 0.05 m respectively. It subjects to the uniform load 1.25 kN/m^2. The Young's modulus of the material is 2×10^9 Pa and the Poisson's ratio is 0.3. Then Young's modulus of the reinforced material is 3×10^{10} Pa and the Poisson's ratio is 0.3,

supported below the shell.

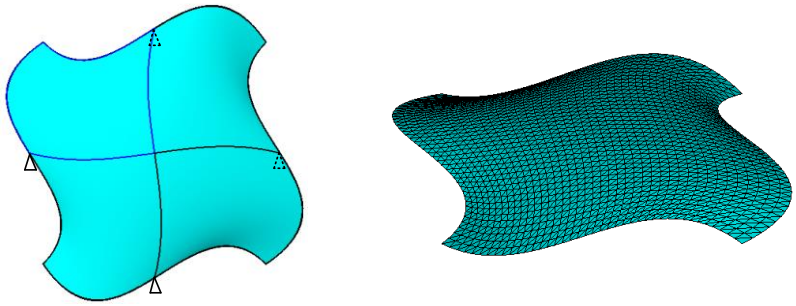

(a) Top view of the model (b) Analysis model with 40×40 elements

Fig. 16. The original shell

The parameterization model of this shell in the shape optimization is constructed by $6\times6\times3$ control points with the order $(3,3,1)$. The topology optimization model has $8\times8\times3$ control points with the order $(2,2,1)$. The control points can be separated by three layers, the two lowest layers control the geometry of reinforced material. The relative position of the two upper layers in the parameterization model is fixed to maintain the topology of the shell. Only a quarter of the control points are taken as optimization variables, due to the 4-fold rotational symmetry (the blue area in Fig. 16. (a)).

During the shape and topology optimization process, the maximum shape change is 3 m and the finite differences equal to 10^{-4}. The maximum volume constraint is 50%. Fig.17 is the geometry of the shell after the 37 steps optimizing. The strain energy of the optimized shell is only 11.63% from the original shell. It is about 34.7% of the shell with the same optimized shape but without the reinforced material. And it is about 85.26% comparing to the shell with the optimized shape and uniform distribution of the reinforced material.

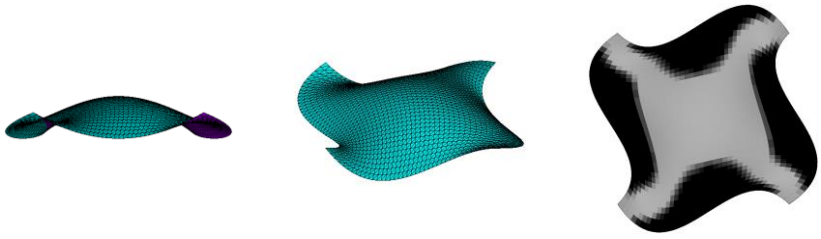

(a) The front view (b) Perspective (c) Reinforced material

contour

Fig. 17. The optimized geometry of the shell

3.4 Example four

In this example, the proposed method is extended to optimize a short thin-walled box with a closed (square) cross-section. Box-shaped structures are generally designed to resist the torsion. The finite model of this structure is shown in Fig. 18. It is fixed at the left edges and subjected to four concentrated loads of 10 kN each, at the right edges. The Young's modulus of the material is 2×10^{9} Pa and the Poisson's ratio is 0.3.

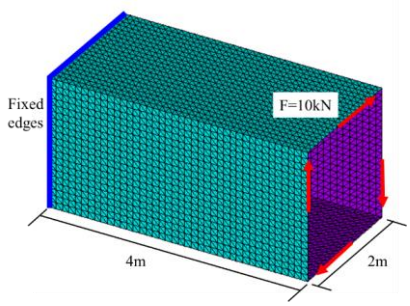

Fig. 18. The finite element model

Four parametric models are created and combined to describe the geometry and topology of this structure. In the shape optimization, only the out-of-plane variation of the control points are taken as the optimization variables. The control points on the boundary edge are fixed during the optimization process. Due to the 4-fold rotational symmetry, only one face of the model is considered during the optimization process. The variations of the other three faces are obtained from the result of the first face. The parametric shape model is constructed by $4\times4\times2$ control points with the order $(3,3,1)$ and the topology optimization model has $8\times8\times2$ control points with the order $(2,2,1)$.

During the optimization, the maximum out-of-plane shape variation is 1 m and maximum material proportion is 50%. The finite differences equal to 10^{-4}. The optimization result after 126 iterations is shown in Fig. 19. The total strain energy is reduced from 236.5 Nm to 74.8 Nm. In the optimized structure, the shape is slightly twisted and the members are nearly 45° on each face which present the truss-like system.

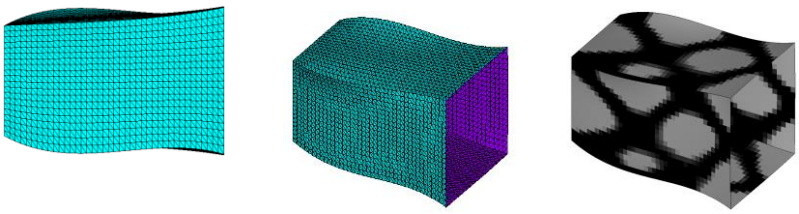

(a) The front view (b) Perspective (c) Optimized topology

Fig. 19. The optimized result of the boxed-shape structure

Moreover, another structure with the length 6 m are optimized. With the frame work, within the proposed method, only the X-direction coordinates of control points need to be changed. It is convenient to design the similar type of structures. The optimization result is shown in Fig. 20. The section of the free edge is enlarged and the twisting is reduced. The strain energy is reduced from 583.13 Nm to 151.87 Nm.

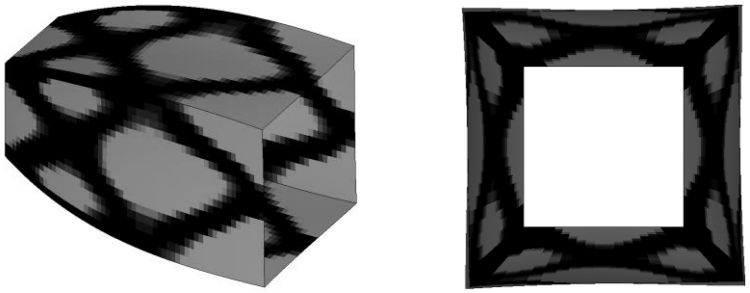

(a) Perspective (b) Front view

Fig. 20. The optimized result

3.5 Discussions

In this part, more numerical examples are tested and compared to illustrate the detailed characteristics of the proposed method. The parameters of the examples are similar with the previous examples in Section 3.1 and 3.2.

3.5.1 The verification of the variable independence

In this section, the independence of the shape variables and topology variables are discussed. Based on the model of two examples, the results of three different variable scaling schemes are compared. Apart from ~~considering~~ the selected scheme of scaling optimization variables, the optimization conditions of the compared cases are all the same ~~with~~ within ~~two~~ both examples,

including ~~such as~~ the analysis loads, boundary conditions~~ies~~, parameterization models and~~,~~ parameters of the MMA method ~~and so on~~. The first scheme is without scaling variables. The second one uses scaled variables, the scal~~inged~~ scheme is ~~introduce~~ explained ~~in the~~ below. The last one considers that the shape variable and the topology variable are independent. In the last case, the shape variables and the topology variables are updated in the MMA optimizer separately. Based on the concept in [25], the scaling of the variables is based on the ~~the~~ scaling factors *kk* which is the ratio of the largest difference of the shape and topology optimization variables, shown in Eq.(11). In the equation, $\mathbf{T}_{max}$ and $\mathbf{T}_{min}$ are upper and lower boundaries of topology optimization variables, $\mathbf{S}_{max}$ and $\mathbf{S}_{min}$ are boundaries of shape optimization variables. The new topology variables $\mathbf{Z}$ are obtained by scaling the original $\mathbf{T}$ topology variables as $\mathbf{Z} = \mathbf{T} / kk$.

$$kk = \frac{\max(\mathbf{T}_{max} - \mathbf{T}_{min})}{\max(\mathbf{S}_{max} - \mathbf{S}_{min})} \tag{11}$$

The optimization histories for the three schemes based on Example one and Example two are shown in Fig. 21. The results of the three schemes of two examples are nearly the same, for both examples. It denotes that shape variables and topology variables are independent. All the schemes are thus suitable to solve these specific problems. Note that the current paper uses the third scheme.

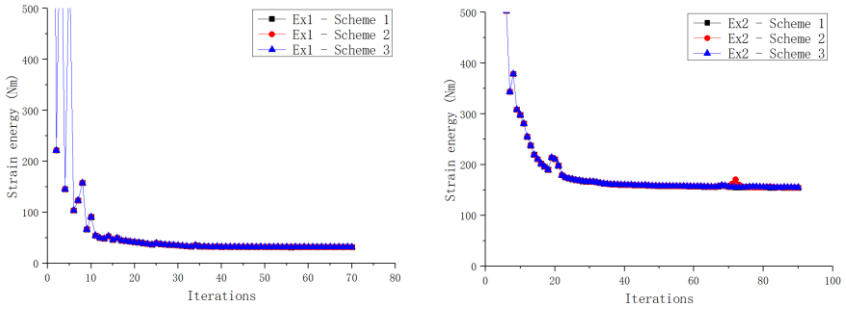

(a) Example one (b) Example two

Fig. 21. Optimization history of three schemes

3.5.2 The necessity of the simultaneous optimization

The simultaneous optimization of shells not only benefits the decreasing of computational costs, but also leads to the more optimized results. In this part, a comparison of the shape and topology

optimization of the two examples is presented, in terms of the simultaneous optimization sequence, the Shape by Topology optimization sequence and the Topology by Shape optimization sequence respectively.

The optimized geometry of the three optimization sequences of the two examples is presented in Fig. 22. It is noticed from the figure that, for the sequence of shape optimization by topology optimization, the two optimized shells has the similar shape with the result of the simultaneous optimization. However, the shape differences lead to an evident difference in the topology result. In the sequence of topology optimization by shape optimization, the topology optimization results are different comparing with the simultaneous optimization result, thus results in the very different optimized shapes of the shells. The results of strain energy are presented in Table 1. The strain energy of the simultaneous optimization sequence is smaller than the obtained energy for the two other sequences. The simultaneous optimization sequence is necessary to obtain a more optimized result.

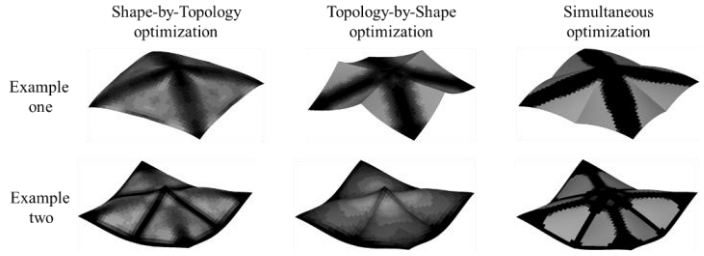

Fig. 22. The optimized results of three optimization sequences

Table 1

Strain energy results (Nm) of three optimization sequences

	Shape-by-Topology	Topology-by-Shape	Simultaneous
Example one	61.30	33.64	31.76
Example two	160.24	278.7	155.1

3.5.3 The impact of using different parameterization models for one problem

The integrated optimization of the shell can proceed with only one parameter model (In this case the number of shape optimization variables remains equal during the topology optimization). However, it may lead to failure and inefficiency in finding the optimized geometry. A comparison with previous results is presented in Fig. 23 to demonstrate the necessity of using the

transformation technique of parameterization models as prescribed in Section 2.2. In the comparison, the optimization parameters and step numbers are similar with the Example two.

In the Fig. 23 the shell optimized by one model with uniformly 4×4 variables shows that it is hard to get the accurate topology optimization result by a small number of variables. Moreover, the result optimized of 7×7 variables shows that the more variables in the shape optimization do not guarantee a better result but may result in a worse one. Usually, due to the increasing nonlinearity of the optimization problem with an increasing number of ~~the~~ shape variables, the difficulty to find optimized results is largely increased.

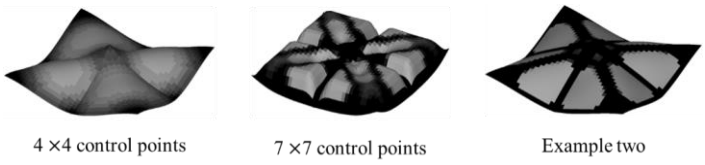

Fig. 23. The comparison of using the different models

The parameterization model gives the flexibility of choosing the number of variables in the optimization process. The optimization results of different numbers of variables are discussed. Next, a comparison based on Example two in which the numbers of topology optimization variables are chosen as 7×7, 9×9 and 11×11. The result is presented in Fig. 24. In figure (a), the shell with more topology variables shows a more detailed optimization results. In figure (b), the strain energy of the results of 7×7, 9×9 and 11×11 variables reduces to 155.1 Nm, 153.14 Nm and 149.27 Nm respectively. With even more variables in the topology optimization, a more optimized result can be obtained, while more computational costs are required.

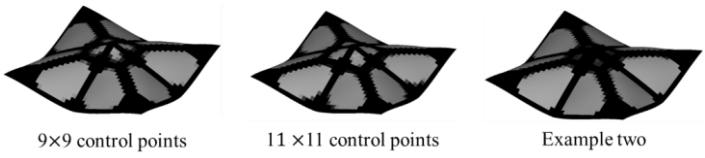

(a) The result after the optimization

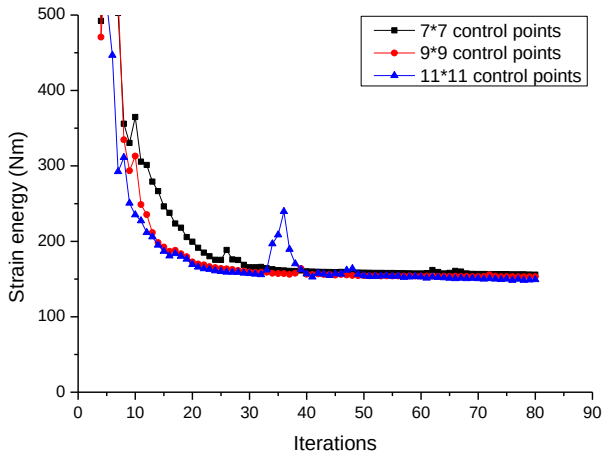

(b) The history of the shape and topology optimization

Fig. 24. The result of different numbers of variables in the topology optimization

3.5.4 The comparison between thickness and topology optimization

In the proposed method, the shape and thickness optimization of the shells can be achieved with a slight change of the parameters during the optimization process. In the thickness optimization, the penalty factor h in the SIMP in the Eq. (9) equals to 1. A comparison of shape-thick optimization and shape-topology optimization of two examples is shown in Fig. 25.

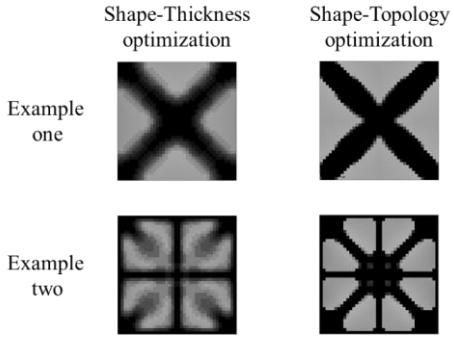

Fig. 25. The geometry of the two kinds of the integrated optimization

In the result of the shape-thickness optimization, the strain energy of the two examples reduce to 24.76 Nm and 135.78 Nm respectively, which are smaller than the results of the shape-topology

optimization (31.76 Nm and 155.1 Nm). Obviously, the thickness optimization is the generation of the topology optimization in the proposed method. After the integrated optimization, the pure membrane state of the shell is approached. The thickness optimization provides more suitable geometry to transform the forces than the topology optimization.

4. Conclusion

In this paper, an integrated optimization method ~~of~~ for simultaneously optimizing shape and topology for free-form shells is proposed.

1. A uniform parameterization model based on NURBS solids with a transformation method is developed to parameterize and optimize the shape and topology of free-form shells. Although shape variables and topology variables are independent in each optimization step, the optimized structure is affected by both.

2. Based on the parameterization model, a small number of variables are used to optimize the free-form shape and topology of the shell, thus simplifying the integrated optimization problem and improving the efficiency. Taking the advantage of the higher continuity of the parameter model, the problem of the formation of checkerboarding patterns and mesh instability in the topology optimization can be prevented.

3. It is noticed from the numerical examples that, the simultaneous optimization sequence is necessary and results in more optimized geometry, compared with the other two optimization sequences (Shape-by-Topology sequence and Topology-by-Shape sequence), while reducing the computational costs.

4. With a little change of the parameters in the method, the shape and thickness optimization problem can be solved instead of the shape and topology optimization. It shows that the shells after shape and thickness optimization have a better structural behavior than the one of the shape and topology optimization. With the development of construction techniques such as 3D printing, free form shells can be designed more efficiently considering thickness optimization.

5. The proposed method gives the flexibility to change the number of variables for parameterizing one shell and leads to the flexible optimization considering both effectiveness and efficiency. Moreover, the method can be utilized to reinforce the free-form shell by considering the reinforced material in the optimization process. Moreover, the method can be extended to optimize more

structures such as the boxed-shaped structures.

Acknowledgments

This work is funded by the NSFC (National Natural Science Foundation of China, a General Program) Project NO. 51378150 and Project NO. 51578186. Yi Xia was supported by the China Scholarship Council for studying at the Delft University of Technology.

Reference

[1] A. Tomás, P. Martí, Shape and size optimisation of concrete shells, Engineering Structures, 32(6) (2010), pp.1650-1658.
https://doi.org/10.1016/j.engstruct.2010.02.013

[2] E. Ramm, W.A. Wall, Shells in Advanced Computational Environment, V World Congress on Computational Mechanics (WCCM5), Vienna, 2002, pp.7-12.
https://scholar.google.nl/scholar?hl=en&as_sdt=0%2C5&q=Shells+in+Advanced+Computational+Environment&btnG=

[3] A. Borgart, A New International Working Group Free-Form Design, 14th SMG Newsletter, IASS—Working Group, No 15, Structural Morphology Group and Sub-working Group on Free-Form Design, 2007.
https://scholar.google.com/scholar?hl=en&as_sdt=0%2C5&q=A+new+international+working+group+free-form+design%2C+14th+SMG+Newsletter&btnG=

[4] F. Otto, B. Rasch, Finding Form: Towards an Architecture of the Minimal, Germany: Edition Axel Menges, 1995.
https://scholar.google.com/scholar_lookup?hl=en&publication_year=1995&author=F.+Otto&title=Finding+Form%3A+Towards+an+Architecture+of+the+Minimal

[5] S. Huerta, Structural design in the work of Gaudí, Architectural Science Review, 49(4) (2006), pp.324-339.
https://doi.org/10.3763/asre.2006.4943

[6] H. Ohmori, K. Yamamoto, Shape optimization of shell and spatial structure for specified stress distribution, Memoirs of the School of Engineering, Nagoya University, 50 (1995), pp.1-32.
http://lib.engg.nagoya-u.ac.jp/seika/kiyou/pdf/50_1L.pdf

[7] K.U. Bletzinger, E. Ramm, Form finding of shells by structural optimization, Engineering

with Computers, 9(1) (1993), pp.27-35.
https://doi.org/10.1007/BF01198251
[8] K.U. Bletzinger, E. Ramm, Structural optimization and form finding of light weight structures, Computers & Structures, 79(22-25) (2001), pp.2053-2062. https://doi.org/10.1016/S0045-7949(01)00052-9
[9] E. Marino, L. Salvatori, M. Orlando, C. Borri, Two shape parametrizations for structural optimization of triangular shells, Computers & Structures, 166 (2016), pp.1-10. https://doi.org/10.1016/j.compstruc.2015.12.008
[10] K.U. Bletzinger, M. Firl, J. Linhard, R. Wüchner, Optimal shapes of mechanically motivated surfaces, Computer Methods in Applied Mechanics and Engineering, 199(5-8) (2010), pp.324-333.
https://doi.org/10.1016/j.cma.2008.09.009
[11] M. Jawad, Theory and design of plate and shell structures, Springer Science & Business Media, 2012.
ISBN: 0412981815
[12] D.C. Lee, J.I. Lee, An integrated design for double-layered structures, Finite Elements in Analysis and Design, 41(2) (2004), pp.133-146.
https://doi.org/10.1016/j.finel.2004.05.002
[13] I. Vizotto, Computational generation of free-form shells in architectural design and civil engineering, Automation in Construction, 19(8) (2010), pp.1087-1105.
https://doi.org/10.1016/j.autcon.2010.09.004
[14] H. Uysal, R. Gul, U. Uzman, Optimum shape design of shell structures. Engineering Structures, 29(1) (2007), pp.80-87.
https://doi.org/10.1016/j.engstruct.2006.04.007
[15] R.J. Yang, A three-dimensional shape optimization system—SHOP3D, Computers & Structures, 31(6) (1989), pp.881-890.
https://doi.org/10.1016/0045-7949(89)90273-3
[16] L. Holzleitner, K.G. Mahmoud, Structural shape optimization using MSC/NASTRAN and sequential quadratic programming, Computers & Structures, 70(5) (1999), pp.487-514.

https://doi.org/10.1016/S0045-7949(98)00179-5

[17] C. Le, T. Bruns, D. Tortorelli, A gradient-based, parameter-free approach to shape optimization, Computer Methods in Applied Mechanics and Engineering, 200(9-12) (2011), pp.985-996.

https://doi.org/10.1016/j.cma.2010.10.004

[18] Y. Okita, T. Honma, Structural morphogenesis for free-form grid shell using genetic algorithms with manipulation of decent solution search, Journal of the International Association for Shell and Spatial Structures, 53(3) (2012), pp.177-184.

https://www.ingentaconnect.com/content/iass/jiass/2012/00000053/00000003/art00009

[19] P. Winslow, S. Pellegrino, S.B. Sharma, Multi-objective optimization of free-form grid structures, Structural and Multidisciplinary Optimization, 40(1-6) (2010), p.257.

https://doi.org/10.1007/s00158-009-0358-4

[20] N. Tanaka, T. Honma, Y. Yokosuka, Structural shape optimization of free-form surface shell and property of solution search using firefly algorithm, Journal of Mechanical Science and Technology, 29(4) (2015), pp.1449-1455.

https://doi.org/10.1007/s12206-015-0317-5

[21] M. Shimoda, Y. Liu, A non-parametric free-form optimization method for shell structures. Structural and Multidisciplinary Optimization, 50(3) (2014), pp.409-423.

https://doi.org/10.1007/s00158-014-1059-1

[22] T. Kimura, H. Ohmori, Computational morphogenesis of free form shells, Journal of the International Association for Shell and Spatial Structures, 49(3) (2008), pp.175-180.

https://www.ingentaconnect.com/content/iass/jiass/2008/00000049/00000003/art00011

[23] R. Ansola, J. Canales, J.A. Tarrago, J. Rasmussen, An integrated approach for shape and topology optimization of shell structures, Computers & Structures, 80(5-6) (2002), pp.449-458.

https://doi.org/10.1016/S0045-7949(02)00019-6

[24] R. Ansola, J. Canales, J.A. Tarrago, J. Rasmussen, On simultaneous shape and material layout optimization of shell structures, Structural and Multidisciplinary Optimization, 24(3) (2002), pp.175-184.

https://doi.org/10.1007/s00158-002-0227-x

[25] B. Hassani, S.M. Tavakkoli, H. Ghasemnejad, Simultaneous shape and topology optimization of shell structures, Structural and Multidisciplinary Optimization, 48(1) (2013), pp.221-233. https://doi.org/10.1007/s00158-013-0894-9

[26] N. Labonnote, A. Rønnquist, B. Manum, P. Rüther, Additive construction: State-of-the-art, challenges and opportunities, Automation in Construction, 72 (2016), pp.347-366. https://doi.org/10.1016/j.autcon.2016.08.026

[27] K. Svanberg, The method of moving asymptotes—a new method for structural optimization, International Journal for Numerical Methods in Engineering, 24(2) (1987), pp.359-373. https://doi.org/10.1002/nme.1620240207

[28] O. Sigmund, J. Petersson, Numerical instabilities in topology optimization: a survey on procedures dealing with checkerboards, mesh-dependencies and local minima, Structural Optimization, 16(1) (1998), pp.68-75. https://doi.org/10.1007/BF01214002

[29] O. Sigmund, N. Aage, E. Andreassen, On the (non-) optimality of Michell structures, Structural and Multidisciplinary Optimization, 54(2) (2016), pp.361-373. https://doi.org/10.1007/s00158-016-1420-7

[30] L. Piegl, W. Tiller, The NURBS book, Springer Science & Business Media, 2012. ISBN: 3540615458

[31] M.P. Bendsøe, N. Kikuchi, Generating optimal topologies in structural design using a homogenization method, Computer Methods in Applied Mechanics and Engineering, 71(2) (1988), pp.197-224. https://doi.org/10.1016/0045-7825(88)90086-2